Variational multiscale turbulence modelling in a high order spectral element method

Thor Gjesdal [*], Carl Erik Wasberg,
Bjørn Anders Pettersson Reif, Øyvind Andreassen

Norwegian Defence Research Establishment (FFI), P.O. Box 25, NO-2027 Kjeller, Norway

Abstract

One of the more promising recent approaches to turbulence modelling is the Variational Multiscale Large Eddy Simulation (VMS LES) method proposed by Hughes et al. [Comp. Visual. Sci., vol. 3, pp. 47-59, 2000]. This method avoids several conceptual issues of traditional filter-based LES by employing a priori scale partitioning in the discretization of the Navier-Stokes equations.

Most applications of VMS LES reported to date have been based on hierarchical bases, in particular global spectral methods, in which scale partitioning is straightforward. In the present work we describe the implementation of the methodology in a three-dimensional high-order spectral element method with a nodal basis. We report results from coarse grid simulations of turbulent channel flow at different Reynolds numbers to assess the performance of the model.

Key words: Large eddy simulation, variational multiscale method, spectral element method, incompressible flow
1991 MSC: 76F65, 65M60, 65M70
PACS: 47.27.Eq, 02.70.Hm, 02.70.Dh

1 Introduction

Large-eddy simulations (LES) provides a physically more appealing framework for turbulent flow prediction than the more traditional Reynolds-averaged

[*] Corresponding author.
  Email addresses: `Thor.Gjesdal@ffi.no` (Thor Gjesdal),
`Carl-Erik.Wasberg@ffi.no` (Carl Erik Wasberg), `Bjorn.Reif@ffi.no` (Bjørn Anders Pettersson Reif), `Oyvind.Andreassen@ffi.no` (Øyvind Andreassen).

models (RANS). In the latter the full impact of the ensemble averaged effect of turbulent advection on the mean flow field has to be modeled. The essence of the LES approach on the other hand is to directly solve (with a complete time and space resolution) the three-dimensional and time-dependent motion of the largest turbulent scales. These scales are in general associated with the most energetic motion of the turbulence field and it is (ideally) only the least energetic motion that need to be modeled. The concept as such is therefore well suited to confront the scale complexity and transient behavior inherent to turbulent flows and offers a more complete representation than RANS models per se.

In traditional LES, large- and small-scale motion are separated by applying a spatial filtering operation to the Navier-Stokes equations. This results in a set of equations for the large-scale motion. The residual motion, i.e. turbulent motions on scales that are smaller than the filter width, appear in these equations as a residual stress term that must be modeled. There are several conceptual issues in filter-based LES that have to be addressed. For instance, filtering and spatial differentiation do not in general commute on bounded domains or for non-uniform grids, and it is not obvious how to prescribe correct boundary conditions for the filtered velocity at solid walls. Another unwarranted character of filter-based LES models is that the residual stress model has a tendency to affect the entire range of the spectrum and not only represent the filtered effect of the unresolved scales near the spectral cut-off. These issues have been the subject of a considerable amount of research, and the lesson learned, in general, is that LES works well in cases where the rate-controlling processes occur at the largest (resolved) scales of motion, or equivalently in flows where the unresolved scales, and consequently the model, only plays a secondary dynamical role.

In this paper we consider a different approach to LES, the variational multi-scale (VMS) LES method originally proposed by Hughes et al. [1]. The VMS LES method employs an a priori scale partitioning in the discretization of the Navier-Stokes equations, instead of filtering to separate the large- and small-scale motion. The scale partitioning appears to overcome some of the disadvantages of filter-based LES. First, since there is no filtering, all issues concerning commutation errors and boundary conditions at solid walls are addressed. Second, since the scale partitioning is performed during discretization, we develop different equations representing different ranges of the spectrum. Different modelling assumptions can then be applied to each range of the spectrum, improving our ability to apply the model terms where they are needed, and only there.

We implement the VMS LES formulation in a high order spectral element method for the solution of the Navier-Stokes equations. Spectral element methods offer an attractive combination of the accuracy of spectral methods and

the flexibility of finite element methods. This provides us with an attractive framework for model development in which the numerical errors can be controlled, such that the true performance of the model can be assessed. The first implementations of the variational multiscale LES method [2,3,4] used global spectral methods. These methods naturally employ an orthogonal modal basis, such that the scale partitioning becomes straightforward. Recently, the method has also been implemented in the context of other numerical schemes, such as finite element methods [5,6] and finite volume methods [7]. Our spectral element code uses an element-wise discretization with nodal basis functions that contain information on all the scales. One of the challenges of the present work is therefore to devise a way to separate the large and the small scales, and to implement the VMS terms. We show that this can be achieved by an element-by-element transformation into the Legendre modal basis functions.

In the following sections we will discuss the variational multiscale method as a turbulence modelling tool, and describe the implementation of the method in a spectral element solver for the incompressible Navier-Stokes equations. Finally we will present computed results, from both a high-resolution DNS and coarse grid VMS LES for the turbulent flow in a plane channel at different Reynolds numbers. The computed results show that, even with simple modelling applied to the small-scale equations, the performance of the methodology is promising.

2   The variational multiscale method

In this section we will discuss the variational multiscale method as a tool for turbulence modelling. The variational multiscale LES method was introduced by Hughes et al. [1] and later elaborated by Collis [8]. We will outline the method following Collis, to shed light on the modelling assumptions employed in the derivation of the model.

The Navier-Stokes equations describing the dynamics of a viscous, incompressible fluid are

$$\nabla \cdot \boldsymbol{u} = 0, \tag{1a}$$

$$\frac{\partial \boldsymbol{u}}{\partial t} + \boldsymbol{u} \cdot \nabla \boldsymbol{u} = -\nabla p + \nu \nabla^2 \boldsymbol{u} + \boldsymbol{f}, \tag{1b}$$

where the independent variables are the velocity, $\boldsymbol{u} = (u, v, w)$, and the pressure, p. The kinematic viscosity is denoted by ν, and $\boldsymbol{f}$ is a body force term. The non-dimensional parameter that characterizes the flow is the Reynolds number $\mathrm{Re} = |\boldsymbol{u}|L/\nu$.

For ease of presentation we assume homogeneous Dirichlet boundary condi-

tions for the velocity, i.e.

$$\boldsymbol{u}(x) = 0 \quad x \in \Gamma.$$

We can then construct the weak, or variational, formulation by choosing test and trial functions in the same function space $\mathcal{V}$. Note however that in general the test and trial spaces will differ at the boundary.

$$U = (\boldsymbol{u}, p) \quad \in \mathcal{V}$$
$$W = (\boldsymbol{w}, q) \quad \in \mathcal{V}$$

We take the inner product of W with Eq. (1) (written in the compact form $\mathcal{N}(U) = F$) to obtain the weak Navier-Stokes operator:

$$(W, \mathcal{N}(U)) \equiv \mathcal{L}(W, U) - \mathcal{R}(\boldsymbol{w}, \boldsymbol{u}) = (W, F), \tag{2}$$

comprising the linear Stokes operator

$$\mathcal{L}(W, U) \equiv (\boldsymbol{w}, \frac{\partial \boldsymbol{u}}{\partial t}) - (\nabla \cdot \boldsymbol{w}, p) + (\nabla^s \boldsymbol{w}, 2\nu \nabla^s \boldsymbol{u}) + (r, \nabla \cdot \boldsymbol{u}), \tag{3}$$

and nonlinear advection represented by the Reynolds projection

$$\mathcal{R}(\boldsymbol{w}, \boldsymbol{u}) = \mathcal{B}(\boldsymbol{w}, \boldsymbol{u}, \boldsymbol{u}), \tag{4}$$

where $\mathcal{B}$ is the tri-linear term.

$$\mathcal{B}(\boldsymbol{w}, \boldsymbol{u}, \boldsymbol{v}) \equiv (\nabla \boldsymbol{w}, \boldsymbol{u}\boldsymbol{v}). \tag{5}$$

To take into account the multiscale representation, we write the solution space $\mathcal{V}$ as a disjoint sum

$$\mathcal{V} = \overline{\mathcal{V}} \oplus \widetilde{\mathcal{V}} \oplus \widehat{\mathcal{V}},$$

in which $\overline{\mathcal{V}}$ and $\widetilde{\mathcal{V}}$ comprise the large and small scales, respectively, whereas $\widehat{\mathcal{V}}$ contains the unresolved scales that cannot be represented by the numerical discretization. The scale partitioning is sketched in Fig. 1. Now, by decomposing the test and trial functions in these spaces

$$U = \overline{U} + \widetilde{U} + \widehat{U},$$
$$W = \overline{W} + \widetilde{W} + \widehat{W},$$

we can develop exact variational equations governing different scales. Furthermore, by assuming that the scale partitioning is orthogonal, we obtain the
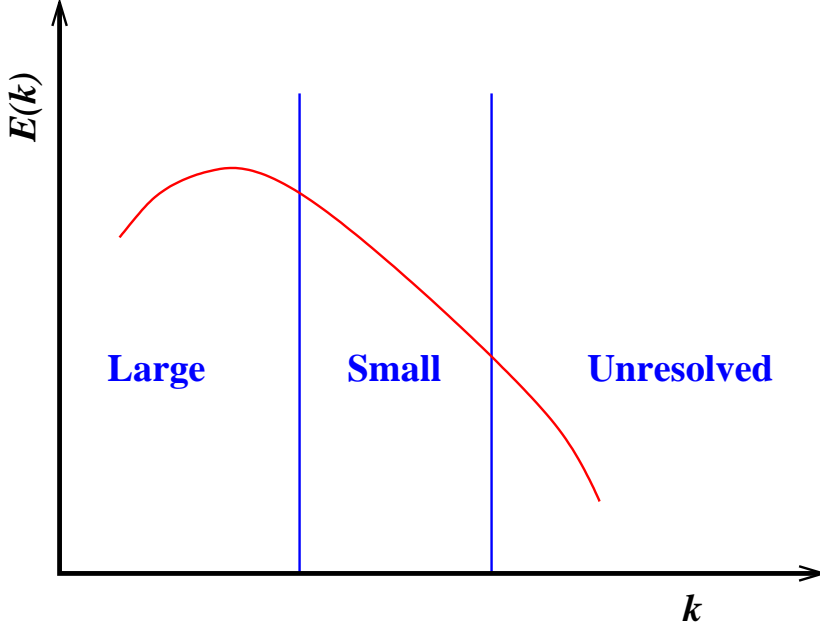
Fig. 1. Schematic of the turbulent energy spectrum with scale partitioning

following equations governing the large, the small, and the unresolved scales:

$$\mathcal{L}(\overline{W},\overline{U}) - \mathcal{R}(\overline{\boldsymbol{w}},\overline{\boldsymbol{u}}) - (\overline{W},F) - \mathcal{R}(\overline{\boldsymbol{w}},\tilde{\boldsymbol{u}}) - \mathcal{C}(\overline{\boldsymbol{w}},\overline{\boldsymbol{u}},\tilde{\boldsymbol{u}})$$
$$= \mathcal{R}(\overline{\boldsymbol{w}},\widehat{\boldsymbol{u}}) + \mathcal{C}(\overline{\boldsymbol{w}},\overline{\boldsymbol{u}},\widehat{\boldsymbol{u}}) + \mathcal{C}(\overline{\boldsymbol{w}},\tilde{\boldsymbol{u}},\widehat{\boldsymbol{u}}), \tag{6a}$$

$$\mathcal{L}(\widetilde{W},\widetilde{U}) - \mathcal{R}(\tilde{\boldsymbol{u}},\tilde{\boldsymbol{u}}) - (\widetilde{W},F) - \mathcal{R}(\tilde{\boldsymbol{u}},\overline{\boldsymbol{u}}) - \mathcal{C}(\tilde{\boldsymbol{u}},\overline{\boldsymbol{u}},\tilde{\boldsymbol{u}})$$
$$= \mathcal{R}(\widetilde{\boldsymbol{w}},\widehat{\boldsymbol{u}}) + \mathcal{C}(\tilde{\boldsymbol{u}},\overline{\boldsymbol{u}},\widehat{\boldsymbol{u}}) + \mathcal{C}(\widetilde{\boldsymbol{w}},\tilde{\boldsymbol{u}},\widehat{\boldsymbol{u}}), \tag{6b}$$

$$\mathcal{L}(\widehat{W},\widehat{U}) - \mathcal{R}(\widehat{\boldsymbol{w}},\widehat{\boldsymbol{u}}) - \mathcal{C}(\widehat{\boldsymbol{w}},\overline{\boldsymbol{u}},\widehat{\boldsymbol{u}}) - \mathcal{C}(\widehat{\boldsymbol{w}},\tilde{\boldsymbol{u}},\widehat{\boldsymbol{u}})$$
$$= \mathcal{R}(\widehat{\boldsymbol{w}},\overline{\boldsymbol{u}}) + \mathcal{R}(\widehat{\boldsymbol{w}},\tilde{\boldsymbol{u}}) + \mathcal{C}(\widehat{\boldsymbol{w}},\overline{\boldsymbol{u}},\tilde{\boldsymbol{u}}) + (\widehat{W},F), \tag{6c}$$

where $\mathcal{C}(\boldsymbol{w},\boldsymbol{u},\boldsymbol{u}') = \mathcal{B}(\boldsymbol{w},\boldsymbol{u},\boldsymbol{u}') + \mathcal{B}(\boldsymbol{w},\boldsymbol{u}',\boldsymbol{u})$ is the cross stress term. We have written these equations in a form such that all terms that depend on the unresolved scales are collected in the right-hand sides. It is thus evident that there is an effect of the unresolved scales on the computable, resolved scales, and it goes without saying that this effect must be modeled. In the original paper by Hughes et al. [1], the modelling assumptions were not stated, but the issue was clarified by Collis [8], who showed that essentially the following assumptions result in a method that is identical to the method proposed by Hughes (which by then had produced excellent results [2,3])

- The separation between large and unresolved scales is sufficiently large so that there is negligible *direct* dynamic influence from the unresolved scales on the large scales.
- The dynamic impact of the unresolved scales on the small scales are on average dissipative in nature.

The simple scalar Smagorinsky-type model is in an averaged sense fully consis-

tent with the last assumption. In order to approximate the temporal behaviour at the cut-off, a more refined modelling approach would be needed. This is however outside the scope of the present study.

With these assumptions, the LES model is only applied to the small scale equation, adding additional dissipation where it is mostly needed. Different implementations of this method by the Hughes group [2,3], by Ramakrishnan and Collis [4], and by Jeanmart and Winckelmans [9] have produced very good results even for wall-bounded channel flows.

We remark here that both assumptions are, or at least should be, open to scrutiny. Firstly, although it is plausible that the unresolved scales do not influence the large scales, it is not necessarily obvious. In fact, a recent analysis by Oberai et al. [10] showed that the energy transfer from the large and small scales, respectively, to the unresolved scales depends critically on the discretization method and the function spaces that are used to perform the scale partitioning. Furthermore, Reynolds number effects or other aspects of the flow physics may mandate that a more sophisticated model for the large scales must be taken into account. Secondly, the assumption of a one-way cascade from the small to the unresolved scales require that flow is properly resolved, such that the cut-off is far out in the inertial range. This is unfortunately not always the case in LES computations. Such considerations are, however, outside the scope of the present study. Our objective is to present an implementation of the VMS LES formulation in the spectral element method. For this purpose the assumptions employed to date [1,8] are acceptable. At present, we merely note in passing that the VMS method presents an excellent framework for improved modelling to address these issues.

Bearing the above in mind, we can formulate the variational modeled equations. The effect of the unresolved scales on the large scales, given by the right-hand side of (6a), is neglected according to the first assumption, while the effect of the unresolved scales on the small scales, given by the right-hand side of (6b), is modeled by a Smagorinsky term. The equation for the unresolved scales is naturally omitted. The resulting set of equations is

$$\mathcal{L}(\overline{W},\overline{U}) - \mathcal{R}(\overline{w},\overline{u}) - \mathcal{R}(\overline{w},\widetilde{u}) - \mathcal{C}(\overline{w},\overline{u},\widetilde{u}) - (\overline{W},F) = 0, \qquad (7a)$$

$$\begin{aligned} \mathcal{L}(\widetilde{W},\widetilde{U}) - \mathcal{R}(\widetilde{w},\overline{u}) - \mathcal{R}(\widetilde{w},\widetilde{u}) - \mathcal{C}(\widetilde{w},\overline{u},\widetilde{u}) \\ - (\widetilde{W},F) = -(\nabla^s\widetilde{w}, 2\nu_T\nabla^s\widetilde{u}). \end{aligned} \qquad (7b)$$

The terms that couple the different scales are evident in (7); the small-scale equation has been supplemented with a dissipative term that accounts for the interactions between the small and the unresolved scales, whereas large-scale Reynolds and cross stress projection account for the large-scale influence on the small scales. The large-scale equation contains a projection of the small-

6

scale Reynolds stress onto the large-scale to account for interaction between the small and the large scales (i.e. back-scatter).

We are however chiefly concerned with the complete resolved solution $\overline{\overline{U}} = \overline{U} + \tilde{U}$, not with the large and small scales per se, and adding the large- and small-scale equations we obtain

$$\left(\overline{\overline{W}}, \mathcal{N}(\overline{\overline{U}})\right) + (\nabla^s \widetilde{\boldsymbol{w}}, 2\nu_T \nabla^s \widetilde{\boldsymbol{u}}) = (\overline{\overline{W}}, F). \tag{8}$$

We note that in this equation, all the interaction terms between the large and the small scales are accounted for in the advection operator $\mathcal{R}$, which is part of the first term on the left-hand side in (8). The projected cross and Reynolds stress terms that appear in the large- and small-scale equations (7) are therefore mainly important for analysis and turbulence modelling, but need not necessarily impact on the implementation of the method. The variational formulation is hence primarily an analysis tool and a vehicle for developing the VMS methodology. The essential feature of the method is that the turbulence modelling should be confined to the small scales. As long as a suitable scale partitioning can be performed on the solution space, the methodology can in principle be applied to any discretization, as indicated by Hughes et al. [2].

3 Implementation in the spectral element method

In this section we describe the implementation of a VMS LES model in a high-order spectral element method for the solution of the incompressible Navier-Stokes equations.

We will start with a brief discussion of Legendre polynomials and the spectral element basis functions. These concepts are important, both for the description of the basic numerical method as well as for the implementation of the variational multiscale framework that follows. More details about the topics covered in Sections 3.1 and 3.2 can be found in [11].

3.1 Legendre spectral elements

The Legendre polynomials are orthogonal with respect to the unweighted inner product in the function space $L^2(-1, 1)$. The Legendre polynomials are given

by the recurrence relation

$$
\begin{aligned}
L_0(x) &= 1, \\
L_1(x) &= x, \\
L_{k+1}(x) &= \frac{2k+1}{k+1}xL_k(x) - \frac{k}{k+1}L_{k-1}(x), \quad k \geq 1,
\end{aligned}
\tag{9}
$$

where $L_N(x)$ is the Legendre polynomial of degree N.

The Gauss-Lobatto-Legendre (GLL) points $\{\xi_j\}_{j=0}^N$ on $\Lambda = [-1,1]$ are defined as the extrema of the Nth order Legendre polynomial $L_N(x)$, in addition to the endpoints of Λ:

$$
\xi_0 = -1, \xi_N = 1, \quad L'_N(\xi_j) = 0, j = 1, \ldots, N-1, \xi_0 < \xi_1 < \ldots < \xi_N. \tag{10}
$$

Furthermore, the Gauss-Legendre (GL) points $\{\eta_j\}_{j=1}^{N-1}$ on Λ, that are used to represent the pressure in the spectral element method, are defined implicitly by $L_{N-1}(\eta_j) = 0$, i.e. as the zeros of the Legendre polynomials of order $(N-1)$ [12]. Note that the GL points do not include the endpoints of Λ.

The spectral element nodal Gauss-Lobatto-Legendre basis is defined by choosing trial and test functions to be the corresponding Lagrangian interpolants at the Gauss-Lobatto-Legendre (GLL) grid points, constructed as Nth order polynomials such that each function has the property

$$
h_j(\xi_i) = \delta_{ij}, \quad i = 0, \ldots, N. \tag{11}
$$

A function $w(x)$ defined on Λ can then be represented by the interpolating polynomial:

$$
w_h(x) = \sum_{i=0}^N w_i h_i(x), \qquad x \in \Lambda, \tag{12}
$$

where $w_i = w(\xi_i)$ are the function values at the GLL points. Higher-dimensional trial and test functions are constructed as tensor products of these one-dimensional functions. Each velocity component is represented this way on each element, and the global representation is the sum of the representations on all elements.

A Gauss-Legendre nodal basis for the pressure is constructed in an analogous way, only taking into account that we use lower-order polynomials in the basis for the pressure to avoid spurious pressure modes in the solution [13].

3.2   Spectral element Navier-Stokes solver

To solve the Navier-Stokes equations (1) we employ an implicit-explicit time splitting in which we integrate the advective term explicitly, while we treat

the diffusive term, the pressure term, and the divergence equation implicitly. After discretization in time we can write (1) in the form

$$(\alpha I - \nu \nabla^2) \boldsymbol{u}^{n+1} = \nabla p + \boldsymbol{g}(\boldsymbol{f}, \boldsymbol{u}^n, \boldsymbol{u}^{n-1}, \dots), \qquad (13a)$$
$$\nabla \cdot \boldsymbol{u}^{n+1} = 0, \qquad (13b)$$

in which the explicit treatment of the advection term is included in the source term $\boldsymbol{g}$. In the actual implementation we use the BDF2 formula for the transient term,

$$\frac{\partial \boldsymbol{u}}{\partial t} = \frac{3\boldsymbol{u}^{n+1} - 4\boldsymbol{u}^n + \boldsymbol{u}^{n-1}}{2\Delta t} + O(\Delta t^2),$$

which gives $\alpha = 3/2\Delta t$ in (13), while we compute the advective contributions according to the operator-integration-factor (OIF) method [14].

The spatial discretization is based on a spectral element method [13,15]; the computational domain is sub-divided into non-overlapping hexahedral cells or elements. Within each element, a weak representation of (13) is discretized by a Galerkin method in which we choose the test and trial functions from bases of polynomial spaces

$$u_i^h \in P_N(x) \otimes P_N(y) \otimes P_N(z), \qquad (14a)$$
$$p^h \in P_{N-2}(x) \otimes P_{N-2}(y) \otimes P_{N-2}(z). \qquad (14b)$$

The velocity component variables are defined in the Gauss-Legendre-Lobatto basis described above, and they are C^0-continuous across element boundaries. The pressure variable is represented in the Gauss-Legendre basis, and is discontinuous across element boundaries. As we noted above, the unknowns, or dependent variables, in the discrete formulation are the function values of the velocities in the GLL points, and of the pressure in the GL points.

The GLL grid corresponding to the Legendre polynomial of degree N has $(N + 1)$ points. Gauss-Lobatto-Legendre quadrature at the $(N + 1)$ GLL points is exact for polynomials of degree up to $(2N - 1)$. Hence, the computation of the inner products corresponding to the diffusive terms in (1) are calculated exactly, whereas the evaluation of the non-linear advective terms incurs quadrature (aliasing) errors. These errors can be detrimental to the stability of the method and must be controlled. The most fundamental approach to de-aliasing is to perform over-integration [16,17] – that is, to over-sample by a factor 3/2 and calculate the quadrature at this refined grid for the inner products containing non-linear terms. The overhead involved depends on the amount of the total computational time that is originally spent on the advection part, but for the channel flow calculations presented here, over-integration typically leads to an increase of around 20% of computational time.

An alternative, and computationally more efficient approach, is to use polynomial filtering of the solutions as proposed by Fischer and Mullen [18], where

a simple filter operator with negligible computational cost is applied to the solution at every time-step. The effect in the spectral space on each element is to transfer a certain fraction (the filter strength) of the energy on the highest order basis polynomial in each element over to the third-highest order polynomial [19]. By this operation, the pile-up of energy on the highest order polynomial is reduced, while the values at the element boundaries are unchanged. Filter strengths as small as 1–5% can have positive effects on the solution.

For the solution of the discrete system of equations we now introduce the discrete Helmholtz operator,

$$H = \frac{3}{2\Delta t}B + \nu A,$$

where A and B are the global three-dimensional stiffness- and mass matrices; the discrete divergence operator, D; and the discrete gradient operator, G. Appropriate boundary conditions should be included in these discrete operators. This gives the discrete equations

$$H\boldsymbol{u}^{n+1} - Gp^{n+1} = B\boldsymbol{f}, \tag{15a}$$
$$-D\boldsymbol{u}^{n+1} = 0, \tag{15b}$$

where the change of sign in the pressure gradient term is caused by an integration by parts in the construction of the weak form of the problem. This discrete system is solved efficiently by a second order accurate pressure correction method. If we let Q denote an approximate inverse to the Helmholtz operator, given by a scaled inverse of the diagonal mass matrix, the pressure correction method can be written

$$H\boldsymbol{u}^* = B\boldsymbol{f} + Gp^n, \tag{16a}$$
$$DQG(p^{n+1} - p^n) = -D\boldsymbol{u}^* \tag{16b}$$
$$\boldsymbol{u}^{n+1} = \boldsymbol{u}^* + QG(p^{n+1} - p^n), \tag{16c}$$

where u^* is an auxiliary velocity field that does not satisfy the continuity equation, i.e. $D\boldsymbol{u}^* \neq 0$.

The discrete Helmholtz operator is symmetric and diagonally dominant, since the mass matrix of the Legendre discretization is diagonal, and can be efficiently solved by the conjugate gradient method with a diagonal (Jacobi) preconditioner. Whereas the pressure operator DQG is easily computed; it is ill-conditioned. The pressure system is solved by the preconditioned conjugate gradient method, with a multilevel overlapping Schwarz preconditioner based on linear finite elements [20].

3.3 Incorporation of VMS LES in the SEM

The implementations of the variational multiscale LES method reported in [2,3,4] used global spectral methods. These methods naturally employ an orthogonal modal basis, such that the scale partitioning becomes straightforward. Our spectral element code uses on an element-wise discretization based on the Legendre polynomials. The Legendre polynomials offer an orthogonal hierarchical basis. Like the majority of the spectral element community, we do however use a *nodal* basis constructed from the Lagrangian interpolant functions. In this case all the basis functions contains information on all the scales and the scale partitioning is no longer straightforward.

3.3.1 Nodal and modal bases

We have demonstrated above that in the *nodal* Gauss-Lobatto-Legendre basis a function $w(x)$ defined on $-1 \le x \le 1$ can be represented by a combination of the interpolating polynomials, as given by (12). The coefficients in the sum are the function values at the grid points.

An alternative, *modal*, representation is to use an expansion directly in the Legendre polynomials

$$w(\xi) = \sum_{j=0}^{N} c_j \sqrt{\frac{2j+1}{2}}\, L_j(\xi), \tag{17}$$

where the unknowns now are the spectral coefficients c_j. The factor $\sqrt{\frac{2j+1}{2}}$ is used to normalize the basis. The scaled Legendre polynomials represents a natural orthonormal basis, in which it is straightforward to perform the scale partitioning. In this setting, it is natural to associate the low order polynomials with the large scales and the higher order polynomials with the smaller scales.

The nodal and modal bases are related through the linear transformation

$$K\boldsymbol{c} = \boldsymbol{w}, \tag{18}$$

where the entries of the matrix K are given by

$$(K)_{ij} = \sqrt{\frac{2j+1}{2}} L_j(\xi_i),$$

and $\boldsymbol{c}$ and $\boldsymbol{w}$ are the vectors of spectral coefficients and GLL nodal function values, respectively.

Let $N = \overline{N} + \widetilde{N}$, such that $\overline{N}$ is the dimension of the polynomial basis for the large scales and $\widetilde{N}$ is the dimension of the small-scale space. The large-scale
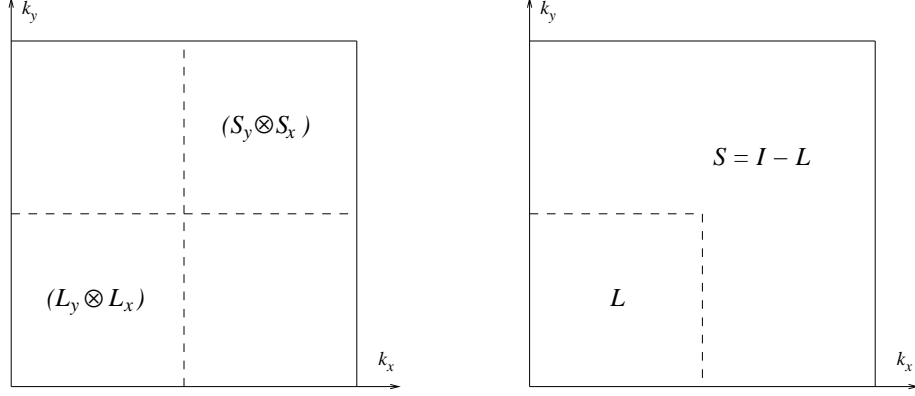
Fig. 2. Large- and small-scale partitions in the 2-dimensional polynomial wavenumber space. The chosen partition operators are shown to the right.

part of a nodal function $\boldsymbol{w}$ can then be written as

$$\widetilde{\boldsymbol{w}} = KTK^{-1}\boldsymbol{w}, \tag{19}$$

where $T = \mathrm{diag}(I_{\widetilde{N}}, 0_{\overline{N}})$ is the operator that annihilates the small-scale components in the modal basis. For notational convenience, we define the large-scale extraction operator

$$L = KTK^{-1},$$

while the corresponding small-scale extraction operator is

$$S = I - L.$$

When tensor products of these operators are formed in higher dimensions, the resulting operators extract the components with large-scale, or small-scale, respectively, components in *all* dimensions. The sum of these two operators does not add up to the identity, so we choose to define the three-dimensional small-scale extraction operator to be

$$S = I - (L_z \otimes L_y \otimes L_x). \tag{20}$$

This is illustrated in two dimensions in figure 2. The resulting small-scale extraction operator returns functions with small-scale structure in *at least one* dimension.

3.3.2   *Properties of the large-small partition*

The large-scale extraction operator corresponds to a sharp cut-off in the Legendre modal space. To illustrate the effect in Fourier space of this large-small partitioning, we represent the function

$$f(x) = \sum_{k=0}^{12} \cos(kx) \tag{21}$$

12
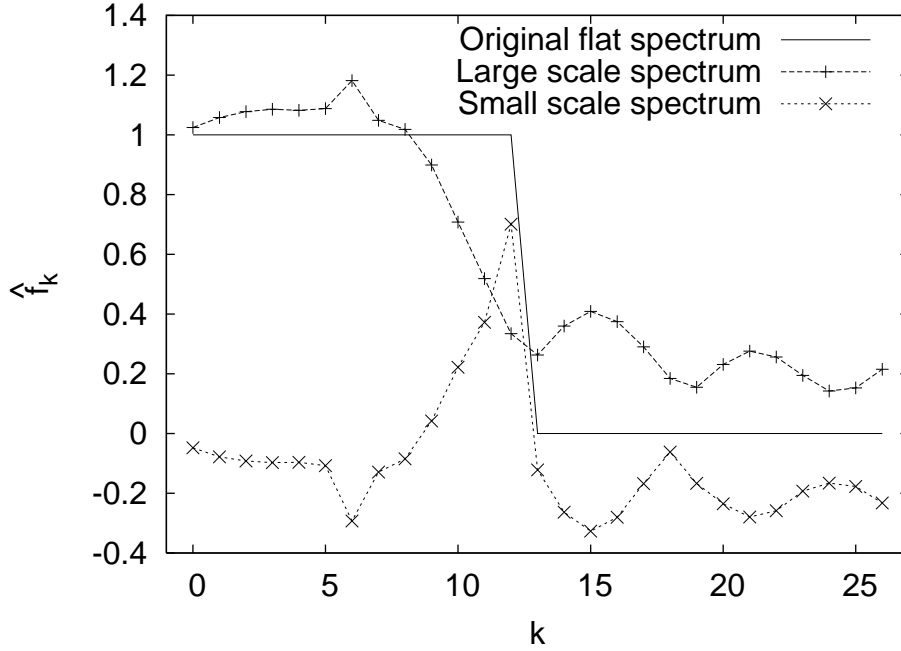
Fig. 3. Fourier representation of a sharp cut-off in Legendre modal space.

on a spectral element grid on $[0, 2\pi]$ with 6 elements and 7 grid points in each element. Higher wave-numbers can not be represented accurately on this particular grid. We extract the large- and small-scale partitions using $\overline{N} = 4$ of the 7 modes (57%) on each element as the large-scale space. The two resulting functions are sampled on a 54-point regular grid, and their Fourier spectra are plotted in figure 3.

The main point illustrated by figure 3 is that although the scale partitioning in the Legendre space is done as a sharp cut-off, the Fourier spectra of the two partitions are much smoother. The reason for this is that each the original cosine terms is represented by a combination of local Legendre modes on each element. We also note that the gradual growth in the small-scale spectrum starts around the cut-off percentage, so the impact of the small-scale extraction is weaker than for a straightforward Fourier representation.

In a more general case with variable element size and/or polynomial order, it may be possible to vary the cut-off point in the local Legendre space to keep the corresponding "average wavelength" approximately constant throughout the whole domain.

3.3.3 Implementation of the model term

We now turn our attention to the implementation of the variational multiscale model term $(\nabla^s \widetilde{\boldsymbol{w}}, 2\nu_T \nabla^s \widetilde{\boldsymbol{u}})$ from (8). Note that the turbulent eddy viscosity ν_T is not a material property of the fluid, but a property of the flow field and

as such varies through the flow domain.

It is instructive to first consider the one-dimensional case with a constant eddy viscosity. Furthermore, for ease of exposition, we only consider a single element. In this case, the weak form of the model term above is

$$\nu_T \int \frac{\partial \widetilde{w}}{\partial x} \frac{\partial \widetilde{u}}{\partial x}. \tag{22}$$

Using the small-scale extraction operator defined above, we have

$$\widetilde{u}(x) = \sum_{m=0}^{N} \sum_{q=0}^{N} S_{mq} u^q h_m(x), \tag{23}$$

and for a given test function on Lagrange form $(w^i(x) = h_i(x))$

$$\widetilde{w}^i(x) = \sum_{p=0}^{N} S_{pi} h_p(x). \tag{24}$$

Inserting these representations and using Gauss-Lobatto quadrature, we obtain

$$
\begin{aligned}
(\nabla \widetilde{w}, \nabla \widetilde{u}) &= \sum_{r=0}^{N} \sum_{p=0}^{N} \sum_{m=0}^{N} \sum_{q=0}^{N} S_{pi} h_p'(\xi_r) S_{mq} u^q h_m'(\xi_r) \rho_r \\
&= \sum_{p=0}^{N} S_{pi} \sum_{m=0}^{N} \sum_{q=0}^{N} S_{mq} u^q \sum_{r=0}^{N} h_p'(\xi_r) h_m'(\xi_r) \rho_r \\
&= \sum_{p=0}^{N} S_{pi} \sum_{m=0}^{N} \sum_{q=0}^{N} S_{mq} u^q A_{pm} \\
&= \sum_{q=0}^{N} (S^T A S)_{iq} u^q = S^T A S u \\
&= (I - L)^T A \widetilde{u},
\end{aligned}
\tag{25}
$$

where the final line is in the form we generalize to higher dimensions. It is easily seen from the second-to-last line that (25) represents a symmetric operator acting on u.

The corresponding term in three dimensions is

$$
\begin{aligned}
(\nabla \widetilde{w}, \nabla \widetilde{u}_i) &= \Big((B^z \otimes B^y \otimes A^x) - (L^{zT} \otimes L^{yT} \otimes L^{xT})(B^z \otimes B^y \otimes A^x) \Big) \widetilde{u}_i \\
&+ \Big((B^z \otimes A^y \otimes B^x) - (L^{zT} \otimes L^{yT} \otimes L^{xT})(B^z \otimes A^y \otimes B^x) \Big) \widetilde{u}_i \\
&+ \Big((A^z \otimes B^y \otimes B^x) - (L^{zT} \otimes L^{yT} \otimes L^{xT})(A^z \otimes B^y \otimes B^x) \Big) \widetilde{u}_i
\end{aligned}
\tag{26}
$$

for each component u_i.

Taking into account that the eddy viscosity, $\nu_T(x, y)$, is not constant but rather a function that varies in space, will distort the tensor product structure of (26). Following the procedure for discretization of terms with variable coefficients described in [11], we can write

$$
\begin{aligned}
(\nabla \widetilde{w}, 2\nu_T(x, y, z)\nabla \widetilde{u}_i) = {} & 2 \left(I^z \otimes I^y \otimes D^{xT} \right) V \left(I^z \otimes I^y \otimes D^x \right) \widetilde{u}_i \\
& - 2 \left(L^{zT} \otimes L^{yT} \otimes (D^x L^x)^T \right) V \left(I^z \otimes I^y \otimes D^x \right) \widetilde{u}_i \\
& + 2 \left(I^z \otimes D^{yT} \otimes I^x \right) V \left(I^z \otimes D^y \otimes I^x \right) \widetilde{u}_i \\
& - 2 \left(L^{zT} \otimes (D^y L^y)^T \otimes L^{xT} \right) V \left(I^z \otimes D^y \otimes I^x \right) \widetilde{u}_i \\
& + 2 \left(D^{zT} \otimes I^y \otimes I^x \right) V \left(D^z \otimes I^y \otimes I^x \right) \widetilde{u}_i \\
& - 2 \left((D^z L^z)^T \otimes L^{yT} \otimes L^{xT} \right) V \left(D^z \otimes I^y \otimes I^x \right) \widetilde{u}_i.
\end{aligned}
\tag{27}
$$

In this equation, D denotes the GLL derivation matrix in each direction. Furthermore, the values of the eddy viscosity are lumped with the GLL integration weights in the diagonal matrix V with the entries $\nu_T^{rst} \rho_r^x \rho_s^y \rho_t^z$, in which rst are the grid point indices and V is ordered to be consistent with the ordering of the element grid points.

We are now finally ready to consider the model term in the form given in (8). Since the product of a symmetric and an anti-symmetric tensor is zero, we find that we only need to to compute the inner product

$$
(\nabla \widetilde{w}, 2\nu_T \nabla^s \widetilde{\boldsymbol{u}}) = \left(\frac{\partial \widetilde{w}}{\partial x_j}, \nu_T \frac{\partial \widetilde{u}_i}{\partial x_j} \right) + \left(\frac{\partial \widetilde{w}}{\partial x_j}, \nu_T \frac{\partial \widetilde{u}_j}{\partial x_i} \right).
\tag{28}
$$

In tensor product form, the VMS small-scale dissipation term for the component of the momentum equation becomes

$$
\begin{aligned}
(\nabla \widetilde{w}, & 2\nu_T(x, y, z)\nabla \widetilde{u}_1) \\
= {} & 2 \left\{ \left(I^z \otimes I^y \otimes D^{xT} \right) - \left(L^{zT} \otimes L^{yT} \otimes (D^x L^x)^T \right) \right\} V \left(I^z \otimes I^y \otimes D^x \right) \widetilde{u}_1 \\
& + \left\{ \left(I^z \otimes D^{yT} \otimes I^x \right) - \left(L^{zT} \otimes (D^y L^y)^T \otimes L^{xT} \right) \right\} V \left(I^z \otimes D^y \otimes I^x \right) \widetilde{u}_1 \\
& + \left\{ \left(D^{zT} \otimes I^y \otimes I^x \right) - \left((D^z L^z)^T \otimes L^{yT} \otimes L^{xT} \right) \right\} V \left(D^z \otimes I^y \otimes I^x \right) \widetilde{u}_1 \\
& + \left\{ \left(I^z \otimes D^{yT} \otimes I^x \right) - \left(L^{zT} \otimes (D^y L^y)^T \otimes L^{xT} \right) \right\} V \left(I^z \otimes I^y \otimes D^x \right) \widetilde{u}_2 \\
& + \left\{ \left(D^{zT} \otimes I^y \otimes I^x \right) - \left((D^z L^z)^T \otimes L^{yT} \otimes L^{xT} \right) \right\} V \left(I^z \otimes I^y \otimes D^x \right) \widetilde{u}_3,
\end{aligned}
\tag{29}
$$

and we obtain similar expressions for the other two components. The couplings between the velocity components, introduced by the second term of (28), are handled by including the cross terms in the explicit part of the time splitting, leaving the Helmholtz problem for the velocity components uncoupled.

As seen from (29), the calculation of the VMS LES model terms requires several additional operations. The increase in total computational work will vary with the size and complexity of the simulation, but for the cases considered in this paper the increase is in the range 20–40%, with the smallest relative increase for the largest simulations. To put these numbers into perspective, we note that the total computational complexity of the spectral element method is $O(K^3N^4)$, so increasing the polynomial order $(N-1)$ from 6 to 7 gives a 70% increase in computational time, about the same as increasing the number of elements in each dimension (K) from 5 to 6 would give.

3.3.4 Smagorinsky model

The eddy viscosity $\nu_T(\boldsymbol{x},t)$ is chosen in [1] as a Smagorinsky-type function:

$$\nu_T = (C_S'\Delta')^2|\nabla^s\widetilde{\boldsymbol{u}}|, \tag{30}$$

or alternatively

$$\nu_T = (C_S'\Delta')^2|\nabla^s\bar{\boldsymbol{u}}|. \tag{31}$$

The former was labeled "small-small" in [2], while the latter was labeled "large-small".

As the purpose of the model term is to approximate the effect of the unresolved scales on the small scales, it is argued in [1] that (30) is more consistent with the physical basis of the method, whereas (31) appears to be a computationally attractive alternative. The results in [2,3] show that good results are obtained with both methods. However, in terms of the spectral element implementation, the "large-small" form is not a computational simplification. A more attractive form is instead the "full-small" term

$$\nu_T = (C_S'\Delta')^2|\nabla^s\boldsymbol{u}|, \tag{32}$$

in which the scale extraction operators are avoided completely.

The sum $|\nabla^s\boldsymbol{u}|$ can be written out as

$$|\nabla^s\boldsymbol{u}| = \sqrt{\frac{1}{2}\sum_{i=1}^{3}\sum_{j=1}^{3}\left(\frac{\partial u_i}{\partial x_j} + \frac{\partial u_j}{\partial x_i}\right)^2}. \tag{33}$$

The constant C_S' is set to 0.1, following [2,3], while Δ' is calculated for each element as the geometric average of the mean grid spacing in each direction.

4 Computational results

4.1 Channel flow

The plane turbulent channel flow is one of the simplest cases of an inhomogeneous turbulence field, and this configuration has therefore been extensively used to assess the performance of turbulence models. The fully developed, statistically stationary, plane channel flow is an equilibrium flow, because there is a global balance between the rate of production of turbulent kinetic energy and the rate of viscous dissipation.

The fluid domain is bounded by two infinitely large parallel solid walls, and the flow is driven by a constant mean pressure gradient in the stream-wise direction along the walls. The boundary conditions are no-slip at the solid walls, and periodicity is imposed in the streamwise (x) and spanwise (z) directions, respectively. The wall-normal direction is thus y, and the channel *half-height* is denoted h.

The instantaneous flow field is three-dimensional and time dependent, the ensemble (or time) averaged flow field is however unidirectional. If we let $\langle \cdot \rangle$ denote the ensemble average, we therefore have $\mathbf{U} = \langle \boldsymbol{u} \rangle = [U(y), 0, 0]$.

The *friction velocity*, u_τ, is defined by

$$u_\tau^2 \equiv \nu \cdot \left. \frac{dU}{dy} \right|_{\text{wall}}, \tag{34}$$

and this is used in the definition of the relevant Reynolds number for plane channel flow: $\mathrm{Re}_\tau \equiv u_\tau h / \nu$.

Integrating the ensemble averaged Navier-Stokes equations in the wall-normal direction yields

$$0 = -\left(\frac{dP}{dx} \right) y + \mu \frac{dU}{dy} - \rho \langle u'v' \rangle, \tag{35}$$

where the pressure gradient is a constant, related to the Reynolds number by

$$-\left(\frac{dP}{dx} \right) = \frac{\mu^2}{h^3} \mathrm{Re}_\tau^2. \tag{36}$$

Hence, the sum of the viscous ($\mu dU/dy$) and turbulent ($-\rho \langle u'v' \rangle$) stresses must vary linearly across the channel. The turbulent stress contribution dominates across the channel except very close to the wall where viscous stress dominates. This region is usually referred to as the viscous sub-layer and its thickness decreases with increasing Reynolds numbers.

	Present DNS	Moser et al.	del Álamo & Jiménez	del Álamo et al.
Re_τ nom.	180	180	550	950
Re_τ act.	178.83	178.13	546.75	934
L_x	8	4π	8π	8π
L_y	2	2	2	2
L_z	4	$\frac{4}{3}\pi$	4π	3π
N_x	112	128	1536	3072
N_y	113	129	257	385
N_z	112	128	1536	2304
Δx^+ mean	12.9	17.7	9.0	8.9
Δy^+ min	0.10	0.054	0.041	0.032
Δy^+ max	8.6	4.4	6.7	7.8
Δz^+ mean	6.4	5.9	4.5	4.5
Elements	16^3	-	-	-
Pol. order	7	-	-	-

Table 1

Grid parameters for the present DNS and the reference simulations by Moser et al. [21] and by del Álamo et al. [22,23]. Grid spacing in wall units are calculated from the nominal Re_τ.

	Coarse-24	Coarse-36	Coarse-42	Coarse-60
Re_τ nom.	180	180	550	950
L_x	8	8	8	8
L_y	2	2	2	2
L_z	4	4	4	4
N_x	24	36	42	60
N_y	25	37	43	61
N_z	24	36	42	60
Δx^+ mean	40.0	60.0	104.8	126.7
Δy^+ min	2.0	4.5	4.6	3.9
Δy^+ max	21.1	29.8	57.4	68.8
Δz^+ mean	20.0	30.0	52.4	63.3
Elements	4^3	6^3	7^3	10^3
Pol. order	6	6	6	6

Table 2

Grid parameters for the VMS LES runs. Grid spacing in wall units are calculated from the nominal Re_τ.

We consider three different Reynolds numbers: $\mathrm{Re}_\tau = 180$, 550, 950, and the VMS LES computations are compared with reference solutions obtained from direct numerical simulations.

18
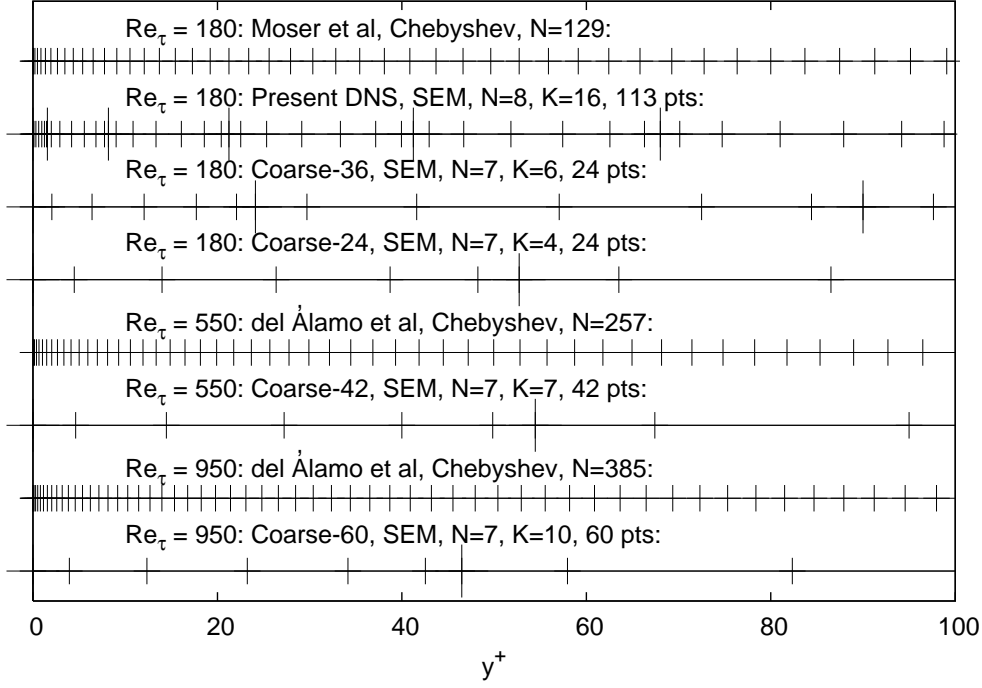
Fig. 4. Details of the point and element distribution in the wall-normal direction for the grids listed in Tables 1 and 2. The longer bars show element boundaries for the spectral element grids.

4.2 Direct numerical simulations at $\mathrm{Re}_\tau = 180$

As a first step towards our ultimate goal, to implement and evaluate the variational multiscale LES method in a high order spectral element flow solver, we performed a Direct Numerical Simulation to verify the code. To this end, we considered fully developed channel flow at $\mathrm{Re}_\tau = 180$, which corresponds to the well-known benchmark simulations reported by Kim et al. [24]. We performed the actual comparison of the results with the updated data set reported by Moser et al. [21] who used a fully spectral Fourier/Chebyshev method with $128 \times 129 \times 128$ grid points.

The simulation was carried out on a computational domain that approximately corresponds to the one used by the reference solutions [21,24], see Table 1 for details. Across the channel we used 16 non-uniformly distributed elements with 8 nodal points in each element. In the streamwise and spanwise directions we used 16×16 uniformly distributed elements with 8×8 nodal points per element. Thus, the total number of nodal points amounts to $112 \times 113 \times 112$ in the streamwise, wall-normal, and spanwise directions, respectively. The solution was advanced in time with a time-step corresponding to 0.18 viscous time-units (ν/u_τ^2), and with 50% polynomial filtering [18] on each time-step. The simulation was initiated by a flow field obtained from

19
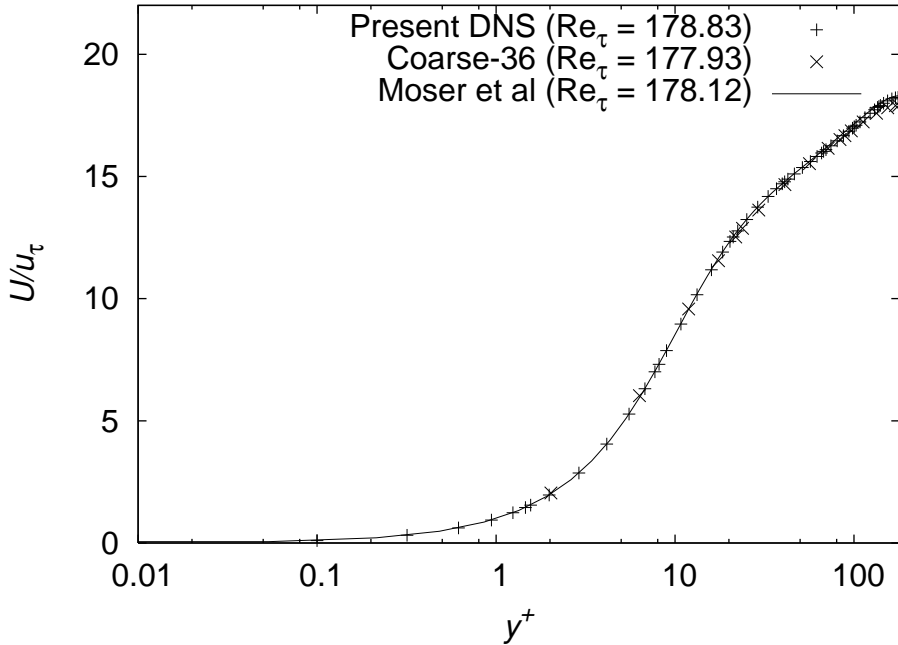
Fig. 5. $Re_\tau = 180$: Variation of the mean velocity across half the channel in viscous units, compared with the reference solution of Moser et al. [21].

an existing plane channel flow solution obtained by a finite-volume code. The flow then evolved approximately 54 flow-through times before a fully developed state was achieved. The results presented here was obtained by collecting statistics over approx. 20 flow-through times. The flow statistics are averaged over the homogeneous – streamwise and spanwise – directions. Homogeneity in a specific direction implies that any correlation of a fluctuating quantities remains invariant under translation in that direction.

4.2.1 Results

The actual computed Reynolds number is $Re_* = 178.83$, i.e. within 0.7% of the prescribed value and well within what can be expected. Moser et al. [21] reported $Re_* = 178.13$. The results presented in Figs. 5–8 compare in all aspects very well with the benchmark data, thus establishing solid confidence in the numerical method. The slight deviations reported herein is well within what should be expected, and even closer correspondence could have been obtained by simply collecting statistics for a longer period of time. This was, however, not considered to be necessary.

As background for the VMS LES results presented below, we also include results from a simulation on the grid "Coarse-36" (see Table 2 for grid properties). This simulation contains no turbulence modelling, but 2% polynomial filtering [18] is employed. Except for the pressure correlations in Fig. 8, the re-
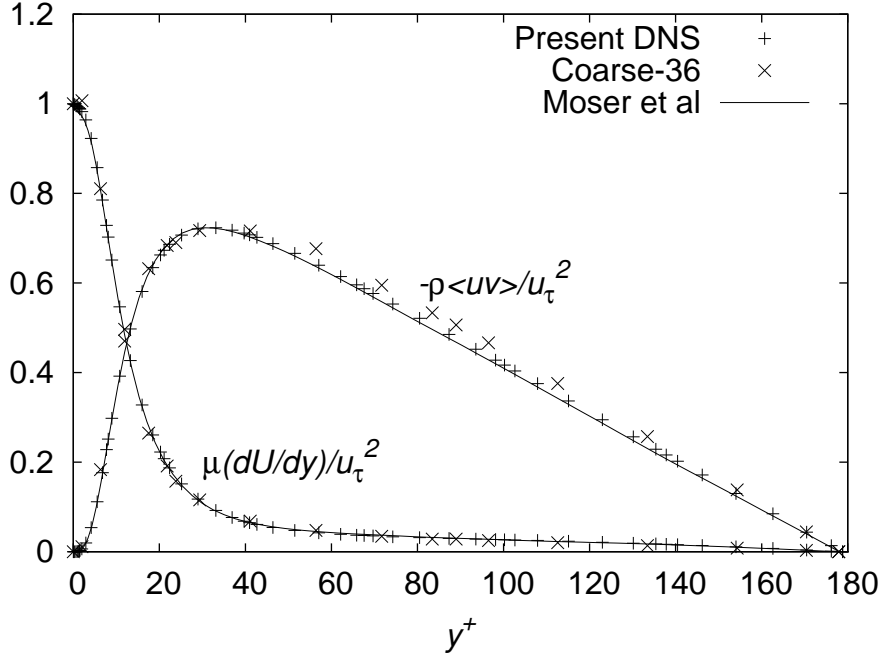
Fig. 6. $Re_\tau = 180$: Variation of mean viscous shear and the turbulent shear stress across half the channel, compared with the reference solution of Moser et al. [21].
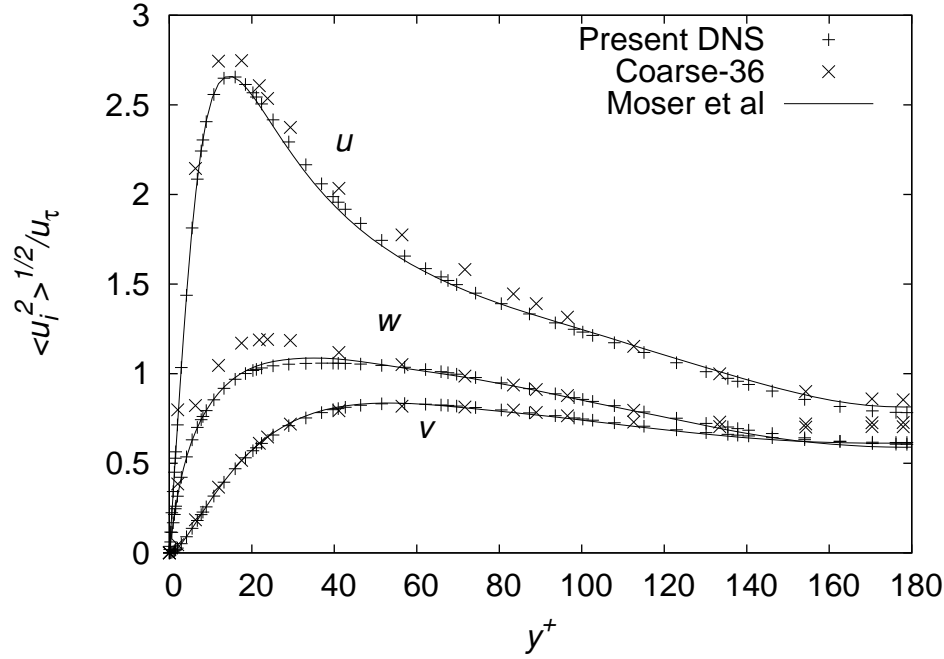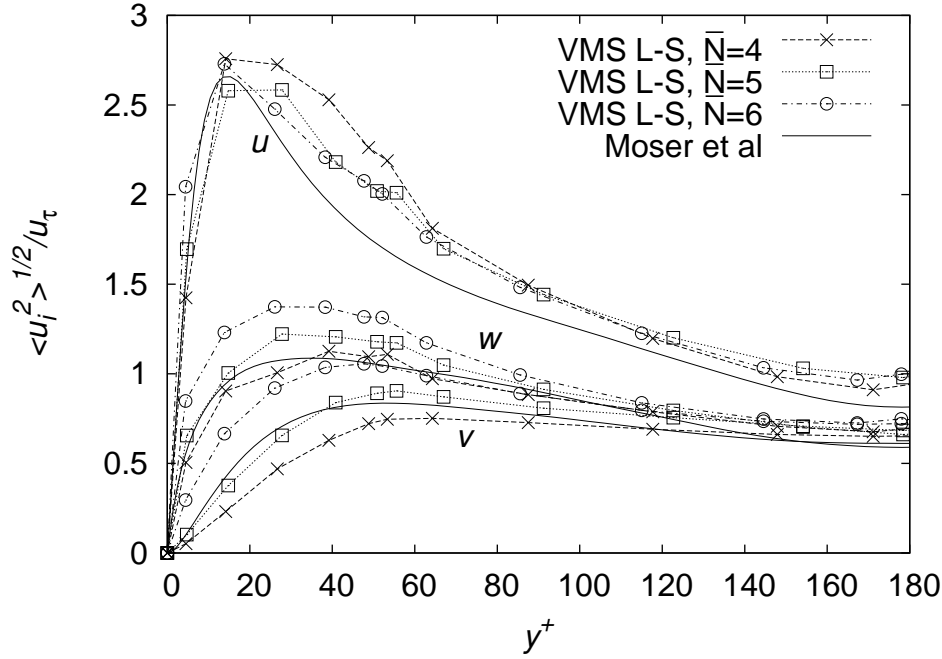

Fig. 7. $Re_\tau = 180$: Variation of streamwise (u'), spanwise (v'), and wall-normal (w') root-mean-square velocity fluctuations across half the channel, compared with the reference solution of Moser et al. [21].
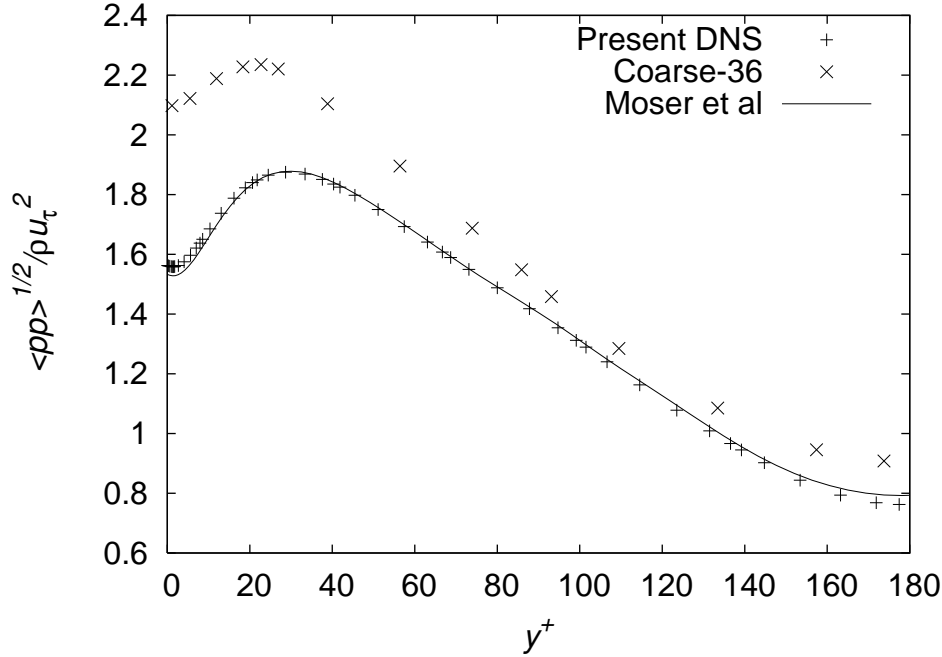
Fig. 8. $Re_\tau = 180$: Variation of the root-mean-square pressure fluctuations across half the channel, compared with the reference solution of Moser et al. [21].

sults are so good that modelling is not expected to improve them. This shows that the spectral element method gives high accuracy even for relatively coarse grids, but it also indicates that plane channel flow is not the most challenging test case. The availability of quality reference data makes it attractive as a starting case, we must however keep in mind that the grids for the model tests have to be sufficiently coarse and not turn into a "quasi-DNS" e.g. near the walls.

4.3 VMS LES results

Lots of combinations of the scale partitioning parameter and the Smagorinsky forms were tested for $Re_\tau = 180$, and the best choice was used for additional simulations at $Re_\tau = 550$ and $Re_\tau = 950$.

The spectral element grid for $Re_\tau = 180$ was chosen as the "Coarse-24" grid described in Table 2. The element interfaces in the wall-normal direction were given by a coarse Gauss-Lobatto-Chebyshev grid, as recommended in [25]. The scale partitioning cut-off mode was kept constant for all elements, even though the element size varied in the wall-normal direction.

In order to get a real test of the modelling, the grid had to be much coarser than what would give reasonably good results without a model. Spectral element grids for the higher Reynolds numbers were constructed such that the first
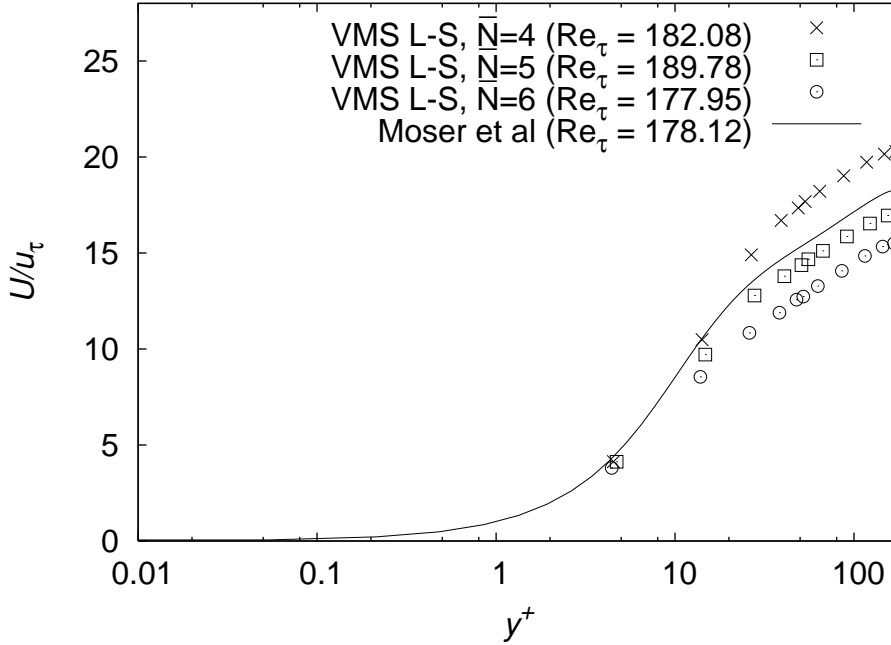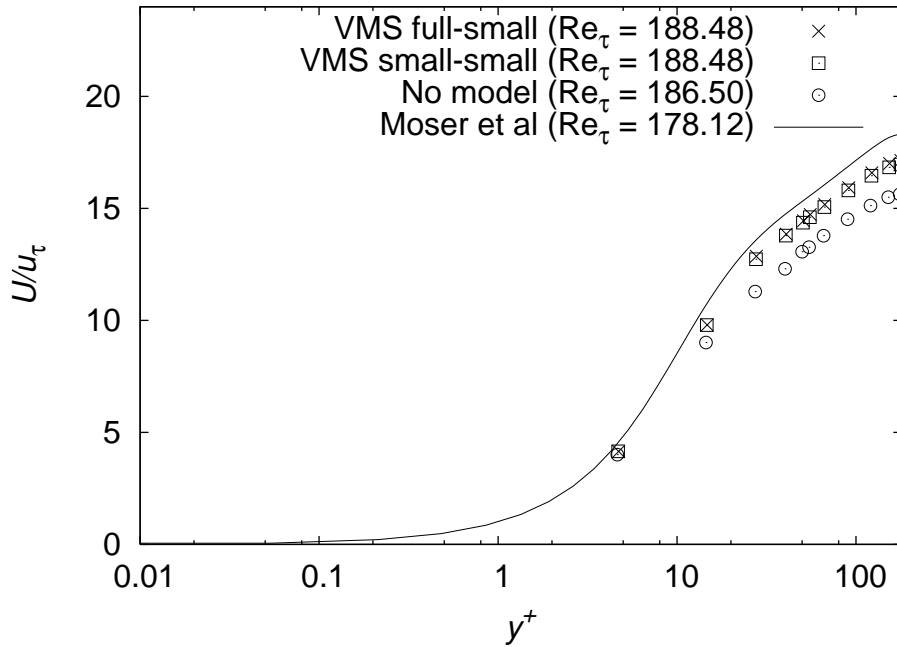
Fig. 9. $Re_\tau = 180$: Variation of the mean velocity across half the channel in viscous units, compared with the reference solution of Moser et al. [21].

element interface in the wall-normal direction is placed at approximately the same value of y^+ for all the cases, see the illustrations in Fig. 4. To reduce the number of parameters, the polynomial degree was fixed for all the VMS LES runs; only the number of elements was changed.

4.3.1 Simulations at $Re_\tau = 180$

The grid parameters for this case are given in the column "Coarse-24" in Table 2.

Without a model, both over-integration and polynomial filtering (2%) was necessary to keep the simulation stable at this resolution. With the VMS model term, either method was sufficient. It was found that polynomial filtering did reduce rather than improve the quality of the results. To obtain the presented VMS results we therefore employed only over-integration in the simulations.

Beside using the different forms of the Smagorinsky term (30)–(32), the scale partitioning was varied in the simulations. With a local grid of 7 grid points in each direction on each element, we have used $\overline{N} = 4$ and $\overline{N} = 5$ for the large-scale extraction described in Section 3.3.1. These values correspond to 57% and 71% of the one-dimensional spectrum, respectively. In three dimensions, the resulting large-scale spaces consist of 19% and 35% of the modes, respectively.

Varying the scale partitioning had a strong influence on the results, and $\overline{N} = 5$

23

Fig. 10. $Re_\tau = 180$: Variation of streamwise (u'), spanwise (w'), and wall-normal (v') root-mean-square velocity fluctuations across half the channel, compared with the reference solution of Moser et al. [21].

Fig. 11. $Re_\tau = 180$: Variation of the mean velocity across half the channel in viscous units, compared with the reference solution of Moser et al. [21].

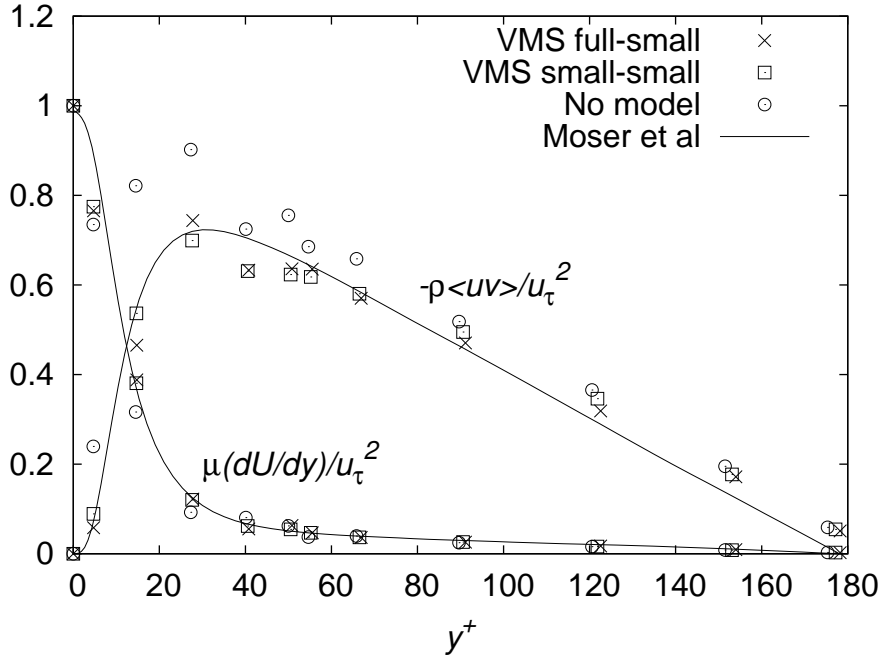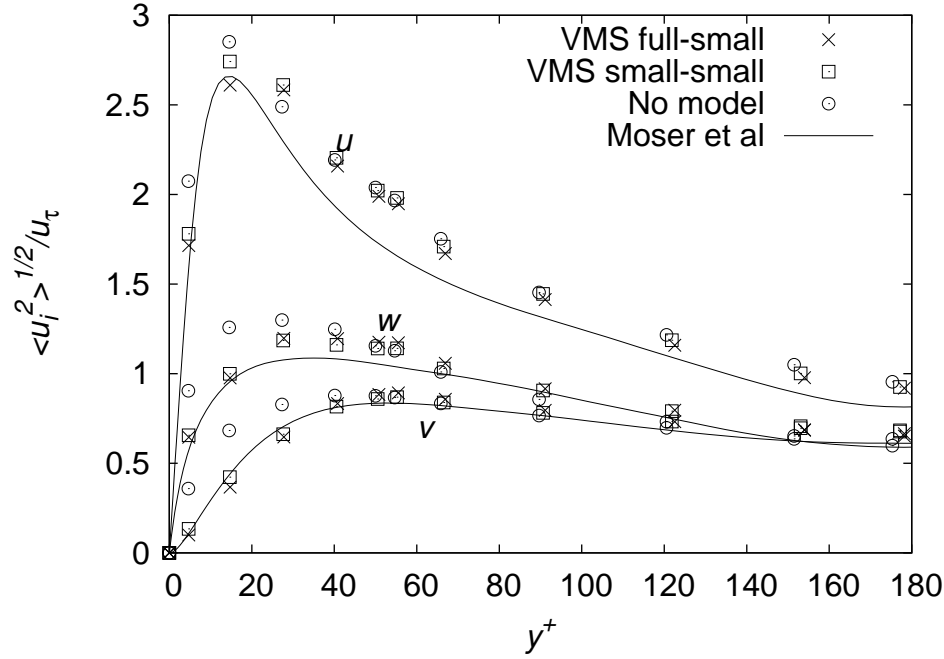was found to be the best choice, as seen from Figs. 9 and 10. The rest of the results shown here are obtained with $\overline{N} = 5$.

Fig. 12. $Re_\tau = 180$: Variation of mean viscous shear and the turbulent shear stress across half the channel, compared with the reference solution of Moser et al. [21].

Fig. 13. $Re_\tau = 180$: Variation of streamwise (u'), spanwise (w'), and wall-normal (v') root-mean-square velocity fluctuations across half the channel, compared with the reference solution of Moser et al. [21].
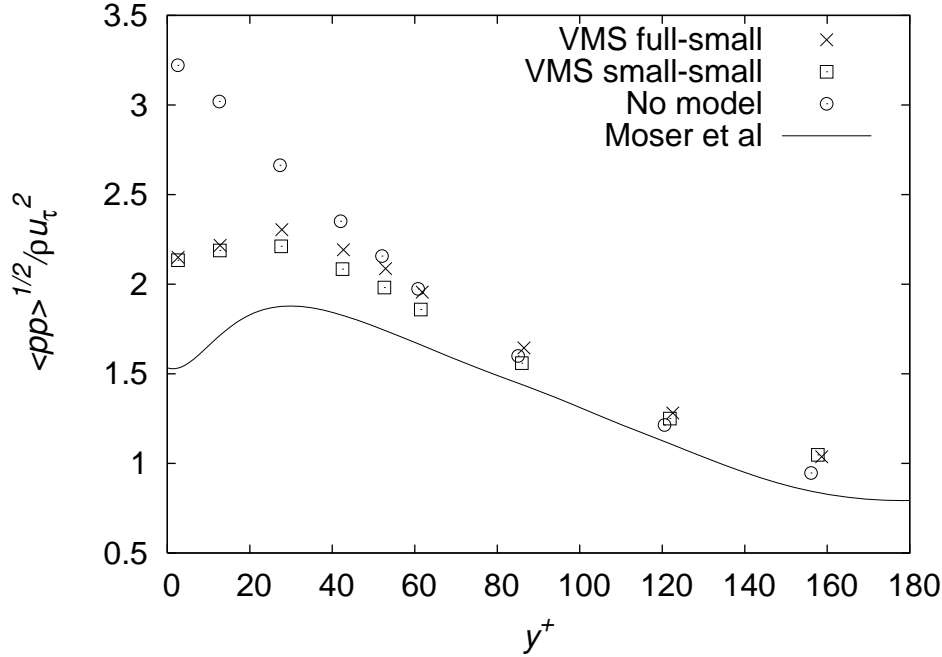
Fig. 14. $\text{Re}_\tau = 180$: Variation of the root-mean-square pressure fluctuations across half the channel, compared with the reference solution of Moser et al. [21].

The different forms of the Smagorinsky term gave very similar results for $\text{Re}_\tau = 180$. The results are presented in Figs. 11–14. The results from "large-small" form (31) were almost indistinguishable from the "full-small" (32) results, and are not included in the figures.

As shown in Section 4.2.1, simulations on the "Coarse-36"-grid gave good results without modelling for this case. Results from simulations without modelling on an intermediate grid with 30^3 grid points were comparable to the VMS results from the 24^3-grid shown here, but at a 40% higher computational cost.

4.3.2   Simulations at $\text{Re}_\tau = 550$

The grid parameters for this case are given in the column "Coarse-42" in Table 2.

The scale partitioning parameter of $\overline{N} = 5$, which was found to be the best choice for $\text{Re}_\tau = 180$, was also used for this case. Again, the "full-small" and "large-small" Smagorinsky forms produced very similar results, so the latter are not shown. The results are presented in Figs. 15–17.
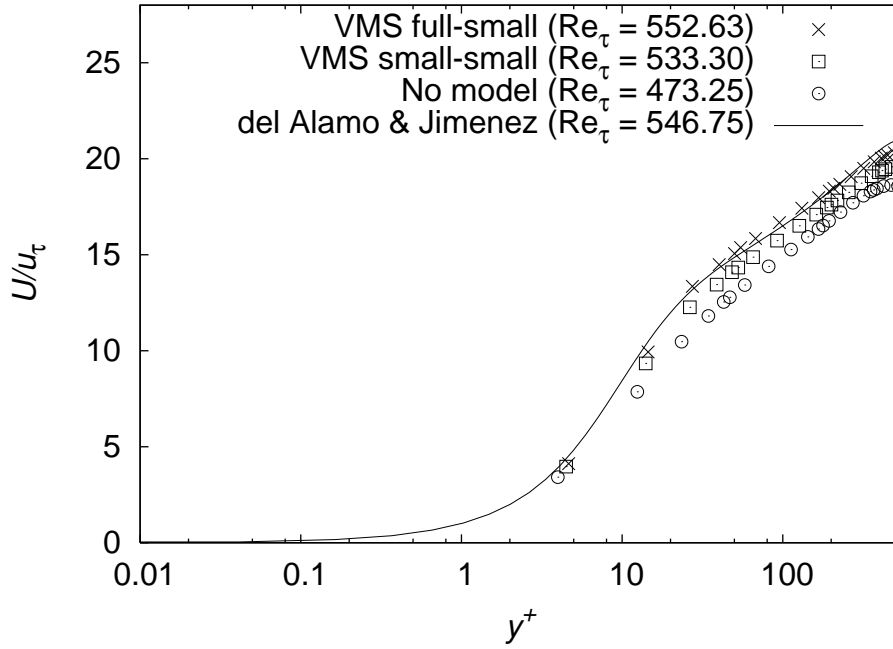
Fig. 15. $Re_\tau = 550$: Variation of the mean velocity across half the channel in viscous units, compared with the reference solution of del Álamo and Jiménez [22].
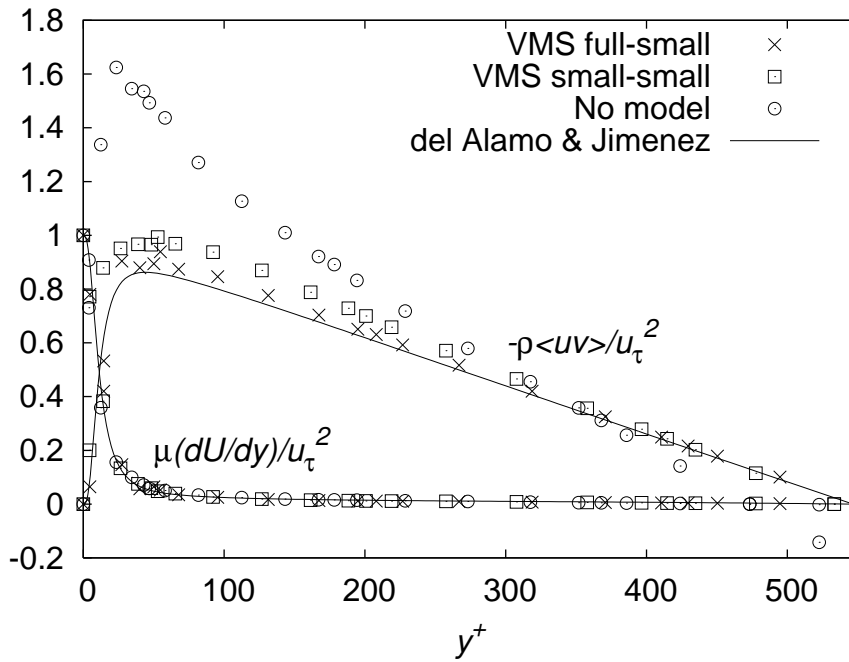

Fig. 16. $Re_\tau = 550$: Variation of mean viscous shear and the turbulent shear stress across half the channel, compared with the reference solution of del Álamo and Jiménez [22].
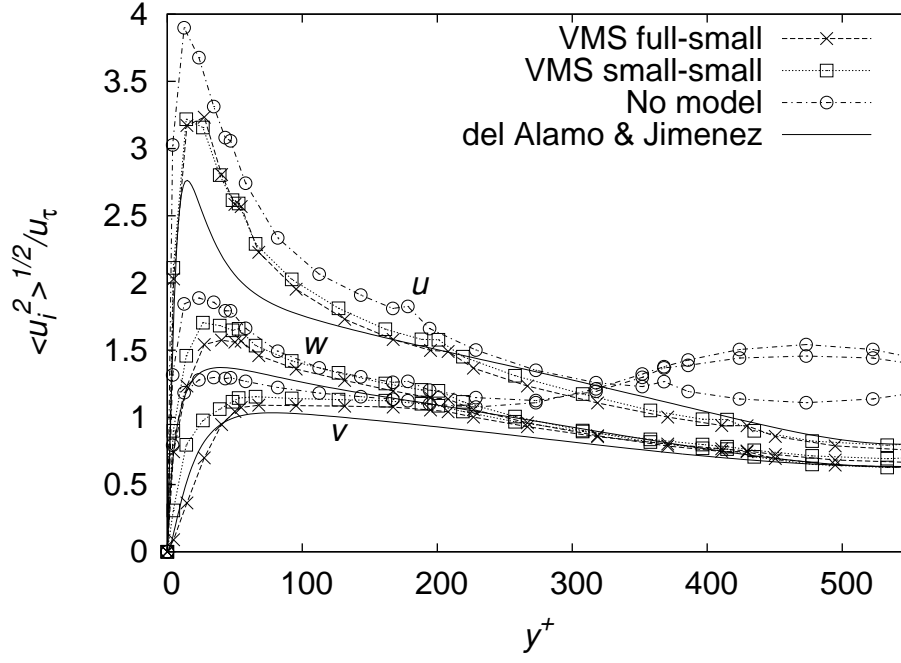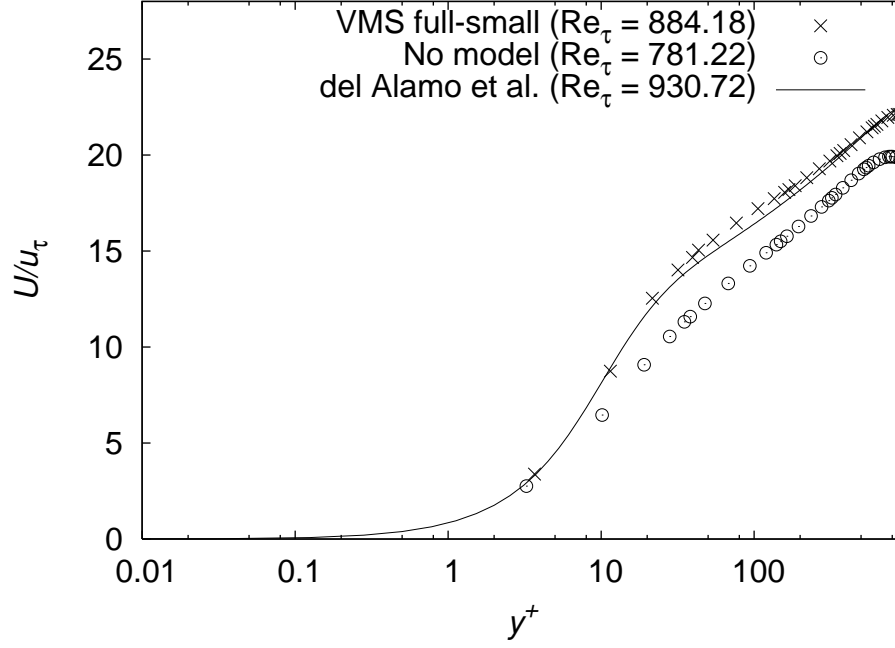
Fig. 17. $Re_\tau = 550$: Variation of streamwise (u'), spanwise (w'), and wall-normal (v') root-mean-square velocity fluctuations across half the channel, compared with the reference solution of del Álamo and Jiménez [22].

Fig. 18. $Re_\tau = 950$: Variation of the mean velocity across half the channel in viscous units, compared with the reference solution of del Álamo et al. [23].
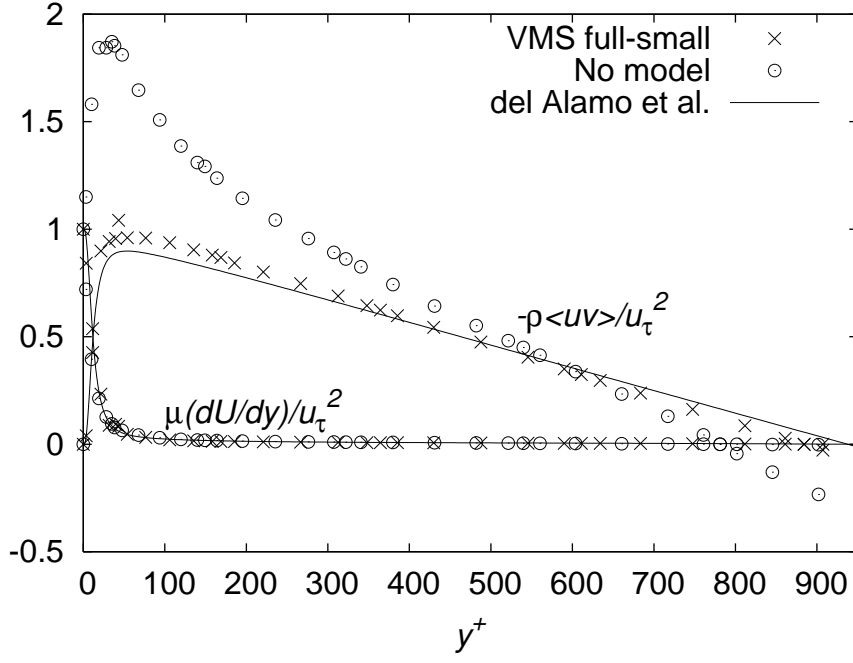
Fig. 19. $Re_\tau = 950$: Variation of mean viscous shear and the turbulent shear stress across half the channel, compared with the reference solution of del Álamo et al. [23].
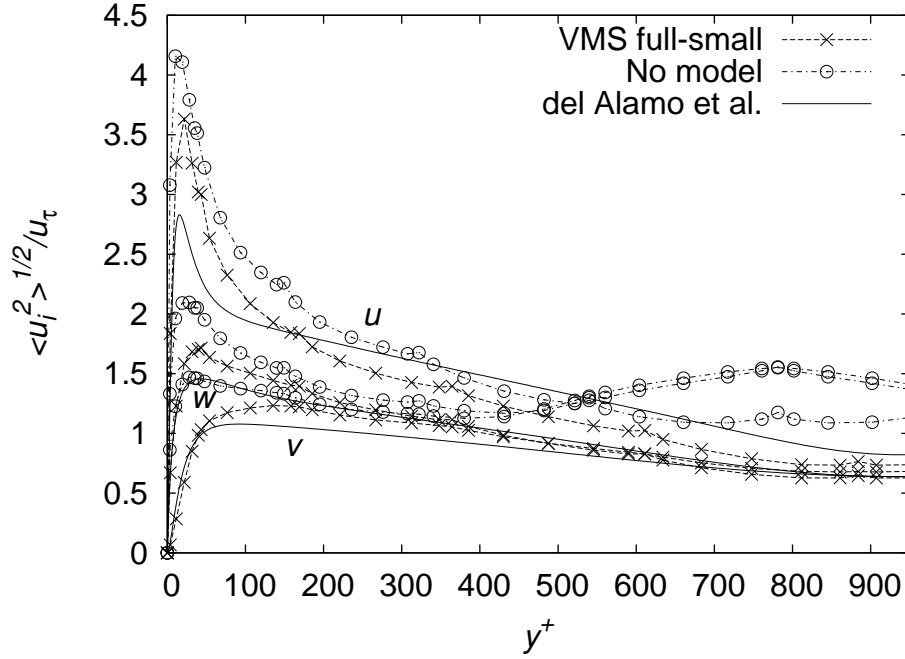

Fig. 20. $Re_\tau = 950$: Variation of streamwise (u'), spanwise (w'), and wall-normal (v') root-mean-square velocity fluctuations across half the channel, compared with the reference solution of del Álamo et al. [23].

29

4.3.3 Simulations at $\mathrm{Re}_\tau = 950$

The grid parameters for this case are given in the column "Coarse-60" in Table 2.

In this case we have only run the "full-small" Smagorinsky form, and the scale partitioning parameter is still $\overline{N} = 5$. The reference simulation is described in [23], and the reference data are downloaded from the site given in [22]. Our results are presented in Figs. 18–20.

4.4 Comments on the results

The VMS LES results show clear improvement from the results without a model, in particular for the higher Reynolds numbers. The plane channel flow at $\mathrm{Re}_\tau = 180$ does not seem to provide sufficient challenges for the testing of turbulence models, as it is too easy to resolve the main features without any modelling at all. The VMS LES results are not compared with alternative turbulence models, as the intentions of this study was mainly to lay the foundations for the incorporation of VMS LES in a spectral element method. Therefore only the simplest Smagorinsky eddy viscosity was used in the model terms in the small-scale equations.

5 Conclusions

The Variational Multiscale Large Eddy Simulation method has been implemented within the framework of a spectral element method. The presented scale partitioning method was shown to produce a gradual introduction of the small-scale model terms. This is intuitively favourable to a sharp cut-off at a given point in the spectral space. The computational overhead for the method was 20–40% for the applications considered here. This must be considered to be reasonably low, as even small increases in the spatial resolution of the spectral element method are more computationally demanding. Good results have been obtained for plane channel flows up to $\mathrm{Re}_\tau = 950$, even for grid densities as low as 0.06% of the reference simulation grid density, and using the simplest possible small-scale dissipation model.

Acknowledgements

References

[1] T. J. R. Hughes, L. Mazzei, K. E. Jansen, Large eddy simulation and the variational multiscale method, Comp. Visual. Sci. 3 (2000) 47–59.

[2] T. J. R. Hughes, L. Mazzei, A. A. Oberai, A. A. Wray, The multiscale formulation of large eddy simulation: Decay of homogeneous isotropic turbulence, Phys. Fluids 13 (2001) 505–512.

[3] T. J. R. Hughes, A. A. Oberai, L. Mazzei, Large eddy simulation of turbulent channel flow by the variational multiscale method, Phys. Fluids 13 (2001) 1784–1799.

[4] S. Ramakrishnan, S. S. Collis, Variational multiscale modelling for turbulence control, AIAA paper 2002-1320 (2002).

[5] V. Gravemeier, W. A. Wall, E. Ramm, A three-level finite element method for the instationary incompressible Navier-Stokes equations, Comput. Methods Appl. Mech. Engrg. 193 (2004) 1323–1366.

[6] V. John, S. Kaya, A finite element variational multiscale method for the Navier-Stokes equations, SIAM J. Sci. Comput. 26 (5) (2005) 1485–1503.

[7] C. Farhat, I. Harari, U. Hetmaniuk, The discontinuous enrichment method for multiscale analysis, Comput. Methods Appl. Mech. Engrg. 192 (2003) 3195–3209.

[8] S. S. Collis, Monitoring unresolved scales in multiscale turbulence modeling, Phys. Fluids 13 (2001) 1800–1806.

[9] H. Jeanmart, G. S. Winckelmans, Comparison of recent dynamic subgrid-scale models in turbulent channel flow, in: Proceedings of the Summer Program 2002, Center for Turbulence Research, NASA Ames/Stanford Univ., 2002, pp. 105–116.

[10] A. A. Oberai, V. Gravemeier, G. C. Burton, Transfer of energy in the variational multiscale formulation of LES, in: Proceedings of the Summer Program 2004, Center for Turbulence Research, NASA Ames/Stanford Univ., 2004, pp. 123–132.

[11] M. O. Deville, P. F. Fischer, E. H. Mund, High-Order Methods for Incompressible Fluid Flow, Cambridge University Press, 2002.

[12] C. Canuto, M. Y. Hussaini, A. Quarteroni, T. A. Zang, Spectral Methods in Fluid Dynamics, Springer-Verlag, 1988.

[13] Y. Maday, A. T. Patera, Spectral element methods for the incompressible Navier-Stokes equations, in: A. K. Noor (Ed.), State of the Art Surveys in Computational Mechanics, ASME, New York, 1989, pp. 71–143.

[14] Y. Maday, A. Patera, E. M. Rønquist, An operator-integration-factor method for time-dependent problems: Application to incompressible fluid flow, J. Sci. Comput. 4 (1990) 263–292.

[15] A. T. Patera, A spectral element method for fluid dynamics: Laminar flow in a channel expansion, J. Comput. Phys. 54 (1984) 468–488.

[16] P. F. Fischer, Private communication, May 2002.

[17] R. M. Kirby, G. E. Karniadakis, De-aliasing on non-uniform grids: algorithms and applications, J. Comput. Phys. 191 (2003) 249–264.

[18] P. F. Fischer, J. S. Mullen, Filter-based stabilization of spectral element methods, Comptes Rendus de l'Académie des sciences Paris, t.332, Série I - Analyse numérique (2001) 265–270.

[19] R. Pasquetti, C. J. Xu, Comments on "Filter-based stabilization of spectral element methods", J. Comput. Phys. 182 (2002) 646–650.

[20] P. F. Fischer, N. I. Miller, H. M. Tufo, An overlapping Schwarz method for spectral element simulation of three-dimensional incompressible flows, in: P. Bjørstad, M. Luskin (Eds.), Parallel Solution of Partial Differential Equations, Springer-Verlag, 2000, pp. 159–180.

[21] R. D. Moser, J. Kim, N. N. Mansour, Direct numerical simulation of turbulent channel flow up to $Re_\tau = 590$, Phys. Fluids 11 (1999) 943–945.

[22] J. C. del Álamo, J. Jiménez, Spectra of the very large anisotropic scales in turbulent channels, Phys. Fluids 15 (6) (2003) L41–L44.

[23] J. C. del Álamo, J. Jiménez, P. Zandonade, R. D. Moser, Scaling of the energy spectra of turbulent channels, J. Fluid Mech. 500 (2004) 134–144.

[24] J. Kim, P. Moin, R. Moser, Turbulence statistics in fully developed channel flow at low Reynolds number, J. Fluid Mech. 177 (1987) 133–166.

[25] G. E. Karniadakis, S. J. Sherwin, Spectral/hp Element Methods for CFD, Oxford University Press, 1999.